Journal of Computational Physics **157,** 89–119 (2000)
doi:10.1006/jcph.1999.6368, available online at http://www.idealibrary.com on IDEAL®

A Compatible, Energy and Symmetry Preserving Lagrangian Hydrodynamics Algorithm in Three-Dimensional Cartesian Geometry

E. J. Caramana, C. L. Rousculp, and D. E. Burton

Applied Theoretical and Computational Physics Division, Los Alamos National Laboratory, MS-D413, Los Alamos, New Mexico 87545
E-mail: ejc@lanl.gov

Received May 17, 1999; revised September 1, 1999

This work presents a numerical algorithm for the solution of fluid dynamics problems with moderate to high speed flow in three dimensions. Cartesian geometry is chosen owing to the fact that in this coordinate system no curvature terms are present that break the conservation law structure of the fluid equations. Written in Lagrangian form, these equations are discretized utilizing compatible, control volume differencing with a staggered-grid placement of the spatial variables. The concept of "compatibility" means that the forces used in the momentum equation to advance velocity are also incorporated into the internal energy equation so that these equations together define the total energy as a quantity that is exactly conserved in time in discrete form. Multiple pressures are utilized in each zone; they produce forces that resist spurious vorticity generation. This difficulty can severely limit the utility of the Lagrangian formulation in two dimensions and make this representation otherwise virtually useless in three dimensions. An edge-centered artificial viscosity whose magnitude is regulated by local velocity gradients is used to capture shocks. The particular difficulty of exactly preserving one-dimensional spherical symmetry in three-dimensional geometry is solved. This problem has both practical and pedagogical significance. The algorithm is suitable for both structured and unstructured grids. Limitations that symmetry preservation imposes on the latter type of grids are delineated.

Key Words: Lagrangian hydrodynamics; symmetry; three-dimensional; fluid dynamics; Cartesian geometry; shock wave simulation.

0021-9991/00

1. INTRODUCTION

Herein is presented a generalization from two dimensions (2D) to three dimensions (3D) of a numerical method for the solution of the equations of fluid dynamics in Lagrangian form that is suitable for the simulation of shock wave dynamics and subsonic, but still compressible, flow speeds. This work is an extension to 3D of the 2D methodology that has been published in four previous papers [1–4]. The framework in terms of which this numerical algorithm is cast is termed "compatible" control volume differencing, as espoused in [1, 5]. The basic idea is that difference operators, such as gradient and divergence, that are used to compute force and work should have to the extent possible the same properties in discrete form as they do in continuum form (for example, negative adjointness). If this is true, then the derivation of other properties, such as conservation of total energy, follow by the same logic in the discrete case as in the continuum one. However, this idea can be made more encompassing in that the above requirements are contained as a subset of what we refer to as "general compatibility." In this case forces can be specified in any manner whatsoever, and the work done by these forces can still be calculated by a generic prescription such that conservation of total energy is always obeyed. This allows for a generalization of the type of forces that can be specified: in particular, artificial viscosity forces [4], and subzonal pressure forces [3]. The Lagrangian formulation of the fluid equations is a powerful adaptive description in that the grid automatically adjusts to follow the moving fluid. The inclusion of an artificial viscosity that is specified only in discrete form, and in conjunction with forces derived from multiple pressures in a zone, allows an accurate and very robust numerical algorithm to be constructed in 3D, as is demonstrated.

A more specific issue that is central in this paper is the development of an algorithm that will preserve perfect one-dimensional (1D) spherical symmetry in 3D Cartesian geometry. This is of crucial importance if meaningful 3D perturbation studies are to be performed with respect to 1D spherical problems. This is a heretofore unsolved numerical difficulty in 3D; the specified solution forms the major part of this work. A precise definition of this problem is first given, and a solution in terms of an appropriate modification of the surface vectors that define control volume differencing is constructed. This is based loosely on previous work [2], but is a significantly new and novel extension.

This paper presents only enough of the material in the first four works cited to make it readable and complete. Section 2 gives the essentials of the form of control volume differencing that we utilize in 3D. This underpins all that follows; the important concepts of a corner mass and a corner force are briefly reviewed. Section 3 gives a discussion of the problem of preserving one-dimensional spherical symmetry in 3D. The kinds of grids on which 1D spherical symmetry can, in principle, be expected to be preserved are discussed. How the gradient operator must be modified from that used in control volume differencing in order that spherical symmetry be preserved is presented in Section 4. Section 5 details how forces are to be discretized to produce a scheme that is both robust and accurate in three dimensions, and preserves 1D spherical symmetry when present, without imposing it when it is not. How this symmetry correction can be efficiently automated so that the underlying control volume scheme is obtained when symmetry is not present is discussed in Section 6. Numerical results are given in Section 7 that demonstrate the effectiveness of the algorithm. This is followed by some final conclusions and an appendix that details the calculation of strain rates.

2. COMPATIBLE CONTROL VOLUME DIFFERENCING, THREE DIMENSIONS

While the ideas and consequences of compatible, control volume differencing on a staggered spatial grid have been given in depth elsewhere [1, 3], the essentials that are needed to frame our discussion are briefly presented in the 3D context. The most basic concepts on a spatially staggered grid, where pressure, density, and internal energy are defined in zone centers, and coordinate position and velocity at the grid points that circumscribe the zones, are that of a corner mass and a corner force. We first define Lagrangian masses by means of the corner mass; corner forces are introduced last.

The corner mass is determined at the initial time by multiplying the zone density by the corner volume. In 2D Cartesian geometry a corner volume is specified as the area delineated by a grid point, the center point of the zone of which it is a part, and the midpoints of the two coordinate lines that intersect the grid point and also form the sides of the given zone. In Fig. 1 the quadrilateral specified by the points *abdea* is a corner area (volume in 3D). The mass inside this volume is the corner mass; we denote the corner mass as m_z^p where the integer indices z and p denote the zone and point, respectively, with which it is associated. These two indices range over all zones and points of the grid. We define $m_z^p = m_p^z$, but always sum the corner mass with respect to the lower index. Now the zonal mass M_z (the mass inside zone z) and the nodal mass M_p (the mass associated with grid point p) are defined in terms of the corner mass as

$$M_z = \sum_p m_p^z, \qquad M_p = \sum_z m_z^p, \tag{1}$$

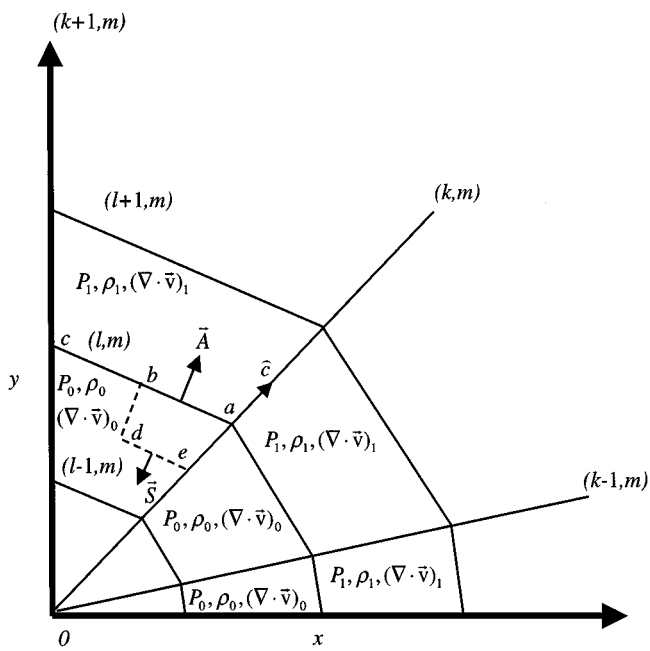

FIG. 1. Planar slice of a 3D logical grid in Cartesian geometry that supports 1D spherically symmetric initial conditions. Quadrilateral *abdea* is a corner area (volume in 3D). Index m denotes third dimension z.

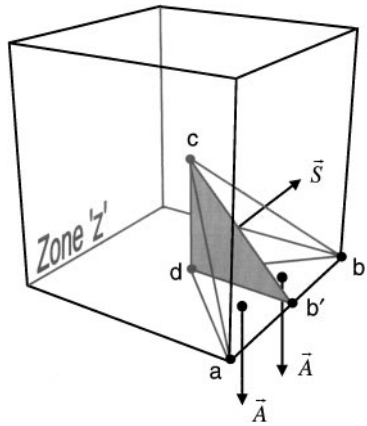

FIG. 2. Tetrahedral decomposition of a hexahedron, used to construct coordinate-line mesh ($\vec{A}$'s), median mesh ($\vec{S}$'s), and corner volumes.

where in the first instance we sum all corner masses with the same index z, and in the second we sum all corner masses with the same index p.

In order to define the corner volume in 2D we must define three auxiliary points: the midpoints of two coordinate lines, and the center point of the zone that is always taken to have coordinates that are the arithmetic average of those that define the zone. In addition, these points are connected by straight lines. (This can be relaxed, as in [6].) However, in 3D not only must appropriate auxiliary points be defined, but surfaces must be fit through more than three points (therefore, not coplanar) in order to compute the surfaces of the zone volumes. The algorithm used here to calculate both volumes and surface area vectors is to tetrahedralize polyhedra of arbitrary order so that the volume of any problem domain can be formed in a general manner on an unstructured grid [5]. For concreteness this is illustrated for the hexahedral zone shown in Fig. 2.

A hexahedral zone is divided into 24 tetrahedra, with two tetrahedra associated with each of 12 edges. One of these tetrahedra is shown in Fig. 2 as described by the points *abcd*. The zone center point c is defined as the average of the coordinates of the eight points that define the hexahedron; the face center point d is defined as the average of the coordinates of the four points that define a hexahedral face. This tetrahedron is exactly bisected to form one with half the original volume as given by points $ab'cd$. This latter tetrahedron is used to compute the following quantities: the vector $\vec{S}$ as the outward normal to the plane of points b', c, d and with the area of this triangle as its magnitude, the vector $\vec{A}$ as the outward normal to the plane of points a, b', d, or b, d, b', and with magnitude of the associated and equal triangular areas. The vector $\vec{S}$ has added to it another vector from the additional tetrahedron located above the one shown (it also contains points a, b, c) to form the vector defined as $\vec{S}_{ba}$, which is the median mesh vector between points a and b of zone z. There are 12 median mesh vectors corresponding to the 12 edges of a hexahedral zone. The vector $\vec{A}$ forms one of the two vector pieces that make up the lower outward coordinate-line mesh vectors of the lower face of points a and b of zone z. For a hexahedral zone there are four such vectors for each of the six faces of a hexahedron, or three vectors from the set $\vec{A}_i$, $i = 1 \cdots 24$, allocated to each point of zone z. (In 2D there are 4 median mesh vectors $\vec{S}_i$, and 8 coordinate-line mesh vectors $\vec{A}_i$, for a quadrilateral zone; one of each is shown in Fig. 1. The volume of tetrahedron $ab'cd$ is found as $\vec{S}_{ba} \cdot \overrightarrow{b'a}/3$, where $\overrightarrow{b'a}$ is the vector from

point a to point b'. This volume is added to the corner volume of both points a and b. For a hexahedron the corner volume thus consists of two such contributions from each of the three edges associated with every point. Therefore, after the 24 tetrahedra of a hexahedral zone are computed as detailed, the median mesh vectors, coordinate-line mesh vectors, and corner volumes are known. (The zone volume is found simply as the sum of all of its corner volumes.) The corner mass m_z^p is then calculated by multiplying the initial corner volume by the zone density; likewise, M_z and M_p follow from Eq. (1). For an unstructured grid composed of arbitrary polyhedra one sweeps all edges of all zones and calculates the above mentioned entities [5]. These fundamental quantities are the building blocks that define the control volume differencing that we employ. The rest of our underlying numerical algorithm is now introduced.

We begin by considering the conservation of total energy. This can be written as

$$\sum_z M_z e_z + \sum_p M_p \vec{v}_p^2/2 = \text{Boundary Work}, \tag{2}$$

where e_z is the specific internal energy of zone z, and $\vec{v}_p$ is the grid point velocity. Thus, the internal and kinetic energies are defined in the zones and at the grid points, respectively. For simplicity we neglect the boundary work term in Eq. (2), and take its time variation as

$$\sum_z M_z \Delta e_z + \sum_p M_p \vec{v}_p \cdot \Delta \vec{v}_p = 0, \tag{3}$$

where Δ denotes the change of a quantity in a discrete time increment. Note that in obtaining Eq. (3) from Eq. (2) we have considered both zone and node masses to be constant.

Next, the force equation at point p can be written as

$$M_p \frac{d\vec{v}_p}{dt} = \vec{F}_p \equiv \sum_z \vec{f}_z^p. \tag{4}$$

In this equation we have defined a new object, $\vec{f}_z^p$, that we call the corner force. This force acts from zone z and is applied to point p such that if one sums all corner forces common to this point (these belong to the neighboring zones that contain this point as a vertex), then the total force acting on point p, $\vec{F}_p$, is obtained. The corner force, like the corner mass, is defined with two indices: one refers to the zone in which it is constructed, and the other indicates the point on which it acts. In our notation, $\vec{f}_z^p = \vec{f}_p^z$, except that we always sum with respect to the lower index. The explicit functional form of the corner force is, as yet, undefined. How these forces are to be computed is discussed in Section 5.

Finally, the rate of work done by corner forces of any functional form (and thus, the change in internal energy due to them) can be computed "compatibly" utilizing conservation of total energy. The main result is that the rate of exchange of kinetic energy from grid point p to zone z due to the corner force $\vec{f}_z^p$ is simply the dot product of this force into the velocity of grid point p. This follows from Eqs. (3), (4) after performing a discrete change of summation by parts and can be rigorously justified [1]. Thus, in general, the change in internal energy produced by the corner forces, $\vec{f}_p^z$, of a given zone z can be calculated by

$$\Delta e_z = -\frac{\sum_p \vec{f}_p^z \cdot \vec{v}_p^{n+1/2} \Delta t}{M_z}, \tag{5}$$

where Δe_z is the change of the specific internal energy of zone z in a time Δt, and $\vec{v}_p^{\,n+1/2}$ is the average of $\vec{v}_p$ at the old and advanced time levels. It is Eqs. (2), (4), (5) that constitute an algebraic identity for an arbitrary functional form of the corner force object, $\vec{f}_z^{\,p}$. This fact allows us to compute the work done by forces that are specified in discrete form in a generic manner utilizing Eq. (5), without the need of a continuum, undiscretized expression for the work they perform. This affords us the freedom needed to specify forces due to an edge-centered artificial viscosity, subzonal pressures, and subzonal deviatoric stress tensors. Operationally, by "compatibility" we mean that the work performed by all forces is computed using Eq. (5).

To complete the system of equations the pressure in a zone, P_z, must be specified. This requires an equation of state, $P_z = P(\rho_z, e_z)$, and thus the zone density ρ_z, as well as e_z from Eq. (5). The zone density is found simply from the zonal mass as

$$\rho_z = M_z / V_z(t), \tag{6}$$

where the zone volume $V_z(t)$ is computed from the zone coordinates at time t, as detailed previously. Initial conditions for ρ_z, V_z, and e_z in the zones, and velocity $\vec{v}_p$ at the points, along with suitable boundary conditions, must be specified.

If Eq. (6) is inserted into the continuity equation that expresses conservation of mass, there results the equation for the evolution in time of a discrete Lagrangian volume element [3, 1]. This equation is

$$(\nabla \cdot \vec{v})_z = \frac{1}{V_z} \frac{dV_z}{dt}, \tag{7}$$

where the volume of a zone z is a function of its defining coordinates $V_z(t) = V_z(\vec{r}_1, \vec{r}_2, \ldots, \vec{r}_n)$; the $\vec{r}_i = \vec{r}_i(t)$ depend on time, and $\vec{v}_i \equiv d\vec{r}_i/dt$ for the motion of a Lagrangian point. What is essential to note is that by defining an explicit functional form for the zone volume in terms of the grid point coordinates, the basic elements of the control volume differencing scheme have been given. This follows from the fact that at the initial time $(\nabla \cdot \vec{v})_z$ is now known directly from Eq. (7). From $V_z(\vec{r}_i(t))$ the grid vectors $\vec{S}_i$ or $\vec{A}_i$ can be derived (we usually work the other way, from surface vectors to volume computation, but these are equivalent), and the grid vectors enable one to construct all discrete forces.

3. THE SYMMETRY PROBLEM

The basic problem in numerically preserving some special one-dimensional symmetry in more than one dimension can be seen simply and intuitively by considering the difficulty with discretizing the pressure forces. A pressure acts normal to any surface, and thus the resulting forces at a grid point depend on the surrounding grid topology. In general, this is arbitrary. Consider a sphere with some constant, nonzero pressure that is allowed to expand freely into an external void. The forces calculated on the discretized initial boundary of the sphere will not point in the radial direction because the net outward normal vector used to compute this force does not generally point radially. Thus, totally numerical deviations from spherical symmetry result. This defective property of the numerical scheme makes the distinction between physical departures from 1D symmetry due to physical perturbations, and departures that are due solely to numerical error, difficult if not impossible to separate.

3.1. *Grid Topology and Restrictions*

It is not possible to achieve spherical symmetry on arbitrarily constructed grids. This is because a prerequisite for symmetry preservation is that a spherically symmetric initial condition be perfectly represented by the initial grid construction; otherwise, numerical perturbations are by necessity present in the initial conditions, and departures from spherical symmetry will always result. In the case where instability is possible they can act to seed its growth.

In Fig. 1 is shown a grid construction in 2D, with coordinate lines that are radial denoted by the logical index k, and those that are angular by the logical index l; the logical index m is common to all points of this figure and is used to denote the third dimension. All points that lie on a line with common index l are at the same distance from the origin 0.

Initial conditions that correspond to spherical symmetry in 3D Cartesian geometry consist of density, specific internal energy, and thus pressure, that must be constant between adjacent lines of index l (referred to as l-lines in 2D and l-surfaces in 3D); and also, the initial velocity must be constant in magnitude (possibly zero) and directed radially on a given l-surface. Two additional requirements must be met. First, $(\nabla \cdot \vec{v})_z$ must be uniform between two l-lines or l-surfaces. From Eq. (7) this implies that the fractional volume change, and thus the density on the next timestep, will remain uniform between l-surfaces. Second, the algorithm for calculating corner volumes, and thus the initial Lagrangian corner masses, must be such that the initial "radially directed" component of the force (computed using unmodified control volume differencing from the initially specified and symmetric pressure), divided by the nodal mass must have a constant magnitude along an l-surface. (The pressure gradient is to be modified so that the tangential component of this force vanish, using the method given in Section 4.) This last requirement places some mild restrictions on the choice of auxiliary points—the center point of a zone and of the zone sides between two l-surfaces in 3D. Generally, defining these points as the arithmetic average of the surrounding dynamical points will allow this requirement (uniform radial acceleration on an l-surface) to be satisfied [2] for a reasonable surface interpolation between these auxiliary points and the dynamical points that define a zone.

If $(\nabla \cdot \vec{v})_z$ satisfies the symmetry requirement this underlying differencing scheme can be modified so that spherical symmetry can be preserved, otherwise it cannot, and is thus not useful for simulating such problems. This is because the procedure presented in the next section that modifies how pressure gradients are computed leaves the original value of $(\nabla \cdot \vec{v})_z$ unchanged for an initially radial velocity field. This procedure modifies only components of the surface vectors that are normal to a locally deduced radial flow direction, denoted as $\hat{c}$. If $(\nabla \cdot \vec{v})_z$ is symmetric the uniform radial acceleration condition mentioned earlier can always be accommodated.

In three dimensions the k-surfaces of Fig. 1 are cones revolved about the vertical z-axis, while the l-surfaces consist of sets of points with the same spherical radius from the origin. If we think of this grid as constructed using spherical coordinates (R, θ, ϕ), these correspond to the logical indices (l, k, m), respectively. However, this type of grid is restrictive; in 3D Cartesian geometry there are many other ways to tessellate a sphere. We wish to use essentially unstructured grids for this purpose, except that they must be able to represent spherical initial conditions exactly. The restriction that this places on our initial grids is that no piece of an l-surface terminate. However, this is very mild. Thus the indices k and m can correspond to a completely unstructured grid with only the l index as a logical

coordinate. Therefore, when spherical symmetry is important, our initial grids consist of sets of points, each set with a common integer index l, that have the same spherical radius initially. Although this permits terminated (k, m) lines, in the rest of this development it is assumed that this in not the case (this situation is discussed elsewhere [7]). Thus, our l-surfaces always consist of the same number of grid points. Although these l-surfaces may be unstructured, they all have the same topology so that each surface can be stretched into every other.

4. MODIFICATION OF THE GRADIENT OPERATOR

Here we present how the gradient operator is to be modified in order that spherical symmetry can be obtained. We are concerned with only that portion of the surface area that is constructed with respect to the logically structured part of the grid where the grid points are separated into logical surfaces, each labelled by the index l. Such a situation is depicted in Fig. 3 where the point "0" is shown connected to its nearest neighbors with solid lines; each of these points has the same surface index l. Although four points that are nearest neighbors to point 0 are shown in Fig. 3, in general the nearest neighbor set associated with any given point will consist of three or more points. This number may vary across the l-surface. The points shown in Fig. 3 as asterisks denote the center points of faces, and the midpoints of edges, of the polyhedra that compose the grid. The coordinates of the face center points are determined as a simple average of those of the surrounding dynamical points with the same logical index l. These points are joined by dashed lines that together with the coordinate line connections form quadrilateral-like subplanes, each with a surface area vector about the point 0 in Fig. 3, and labelled as $\vec{A}_{i,0}$ where $i = 1 \ldots 4$. It is the sum of these vectors about each point of the surface l that is to be modified so that symmetry can be obtained. This is to be done for both the coordinate-surface and the median-surface pieces of the mesh associated with the logical index l in the manner that is detailed next. Then in Section 5 it is explained how forces are to be computed using these modified, directed surface areas.

It is assumed that the points $0 \ldots 4$ all lie on the surface of a sphere of radius a with a center point that has coordinates given by the vector $\vec{R}_{ctr}$ with respect to an arbitrary origin

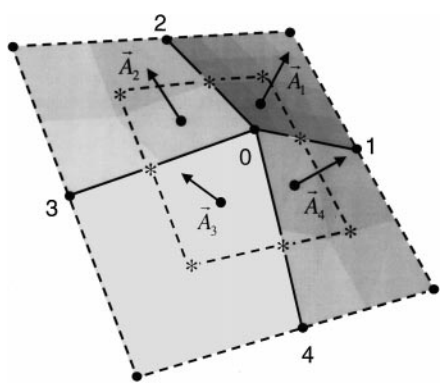

FIG. 3. Coordinate-line mesh about grid point 0 on a logical surface with index l. Solid lines connect nearest neighbor grid points (solid dots). Vectors $\vec{A}_i$ are the piece of the gradient operator that is to be modified about point 0.

of our coordinate system. These two quantities are unique only to the point 0 with its nearest neighbor point set. With respect to some other point on the same l-surface with its nearest neighbor point set these quantities may be completely different. That is, we do not assume any common spherical center point or radius for the points on the logical surface l. What we seek, given only the coordinate locations of the points $0 \ldots 4$ (points $0 \ldots n$ with $n \geq 3$, in general), is the unit vector that points in the outward normal direction to a sphere placed through these points, either directly or in the least squares sense, at the point 0. This we label as the unit vector $\hat{c}$. Then we modify the surface area vectors $\vec{A}_i$ about point 0 such that when summed they yield a net resultant vector that is parallel to the direction $\hat{c}$.

The unit vector $\hat{c}$, thus defined, can be computed as follows: First, the points $0 \ldots n$ have known position vectors given by $\vec{R}_i$, $i = 0 \ldots n$ (although $n = 4$ in Fig. 3, this derivation is kept completely general). Since these points are assumed to lie on the surface of a sphere with center point position vector $\vec{R}_{ctr}$, and with radius a, we have that

$$(\vec{R}_i - \vec{R}_{ctr})^2 = a^2 \qquad \text{for } i = 0 \ldots n. \tag{8}$$

Next point 0 is singled out with respect to its neighbors by writing $\vec{R}_i = \vec{R}_0 + (\vec{R}_i - \vec{R}_0) \equiv \vec{R}_0 + \Delta\vec{R}_{i,0}$ for $i \geq 1$, where the vectors $\Delta\vec{R}_{0,i} = (\vec{R}_i - \vec{R}_0)$ are known coordinate vector lengths. Using this identity in Eq. (8) to replace $\vec{R}_i$ yields

$$(\vec{R}_0 - \vec{R}_{ctr} + \Delta\vec{R}_{i,0})^2 = a^2 \qquad \text{for } i \geq 1. \tag{9}$$

Next we substitute Eq. (8) with $i = 0$ into Eq. (9) above to eliminate the dependence on the spherical radius a^2 to obtain

$$2\Delta\vec{R}_{i,0} \cdot (\vec{R}_0 - \vec{R}_{ctr}) = -(\Delta\vec{R}_{i,0})^2 \qquad \text{for } i \geq 1. \tag{10}$$

This result can be written in matrix form as

$$\mathbf{A}\mathbf{x} = \mathbf{b}, \tag{11}$$

where the ith row of the $n \times 3$ dimensional matrix $\mathbf{A}$ is given by the components of the vector $2\Delta\vec{R}_{i,0} = 2[(x_i - x_0), (y_i - y_0), (z_i - z_0)] \equiv 2[\Delta x_i, \Delta y_i, \Delta z_i]$; the 3×1 column vector $\mathbf{x}$ of the unknowns has components $[(x_0 - x_{ctr}), (y_0 - y_{ctr}), (z_0 - z_{ctr})]$, and the $n \times 1$ inhomogeneous data vector $\mathbf{b}$ has the entries $-(\Delta\vec{R}_{i,0})^2$. If $n > 3$ this system of equations is over-determined. To obtain a unique solution it is multiplied by the transpose of the matrix $\mathbf{A}$, denoted as $\mathbf{A^T}$, to obtain

$$\tilde{\mathbf{A}}\mathbf{x} = \tilde{\mathbf{b}}, \tag{12}$$

where

$$\tilde{\mathbf{A}} \equiv \mathbf{A^T}\mathbf{A} = \mathbf{4}\begin{bmatrix} \sum_i \Delta x_i^2 & \sum_i \Delta x_i \Delta y_i & \sum_i \Delta x_i \Delta z_i \\ \sum_i \Delta y_i \Delta x_i & \sum_i \Delta y_i^2 & \sum_i \Delta y_i \Delta z_i \\ \sum_i \Delta z_i \Delta x_i & \sum_i \Delta z_i \Delta y_i & \sum_i \Delta z_i^2 \end{bmatrix}, \tag{13}$$

$$\tilde{\mathbf{b}} \equiv \mathbf{A^T}\mathbf{b} = -\mathbf{2}\begin{bmatrix} \sum_i \Delta x_i (\Delta\vec{R}_{i,0})^2 \\ \sum_i \Delta y_i (\Delta\vec{R}_{i,0})^2 \\ \sum_i \Delta z_i (\Delta\vec{R}_{i,0})^2 \end{bmatrix}. \tag{14}$$

Here $\sum_i$ has the range $i = 1 \ldots n$ over the l-surface nearest neighbors of point 0. This operation is equivalent to performing a least squares fit of a sphere to the set of points $i = 0 \ldots n$, and thus leads to a 3×3 system of linear equations. The solution vector components x_j are given by $x_j = \det \tilde{\mathbf{A}}_\mathbf{j} / \det \tilde{\mathbf{A}}$, where $\det \tilde{\mathbf{A}}$ is the determinant of the matrix $\tilde{\mathbf{A}}$, and the matrix $\tilde{\mathbf{A}}_\mathbf{j}$ is formed from the matrix $\tilde{\mathbf{A}}$ by replacing the jth column of $\tilde{\mathbf{A}}$ with the column vector $\tilde{\mathbf{b}}$. The jth component of the unit vector $\hat{c}$ that we seek, denoted as c_j, is given by dividing each x_j by the magnitude of the vector $\mathbf{x}$, where $|\mathbf{x}| = (\sum_{\mathbf{j}=\mathbf{1}}^{\mathbf{3}} \mathbf{x}_\mathbf{j}^\mathbf{2})^{\mathbf{1/2}}$. Thus, our final result for the components c_j is

$$c_j = \frac{\det \tilde{\mathbf{A}}_\mathbf{j}}{\left[\sum_{j=1}^{3} (\det \tilde{\mathbf{A}}_\mathbf{j})^\mathbf{2} \right]^{1/2}} \qquad (j = 1, 2, 3). \tag{15}$$

From Eq. (15) it is seen that finding the direction $\hat{c}$ involves only the computation of the determinant of three 3×3 matrices at every grid point. This equation gives the direction cosines of the outward normal to a sphere at the point 0 that is fit to the set of points $i = 0 \ldots n$. If all of these points are coplanar the radius vector $(\vec{R}_0 - \vec{R}_{ctr})$ of this sphere goes to infinity. Suppose all points lie in the x–y plane so that $\Delta z_i = 0$ for all i. Now not only are both the third column and the third row of $\tilde{\mathbf{A}}$ zero, but also the third entry in the vector $\tilde{\mathbf{b}}$. Thus, the matrices $\tilde{\mathbf{A}}_\mathbf{j}$ all have zero determinant and Eq. (15) for the components c_j becomes ill-defined. (Note that this does not occur if we have $i = 3$ and solve for $\mathbf{x}$ from Eq. (11), since then only the third column of $\mathbf{A}$ vanishes and $\mathbf{b}$ has all nonzero entries.)

It is important that $\hat{c}$ never have all zero components or be determined by numerical noise. To prevent this we develop the following procedure. First, note that the trace of $\tilde{\mathbf{A}}$ is never zero since $\mathrm{Tr}(\tilde{\mathbf{A}}) = \sum_\mathbf{i} (\boldsymbol{\Delta} \vec{\mathbf{R}}_\mathbf{i})^\mathbf{2}$. Also, only one eigenvalue of $\tilde{\mathbf{A}}$ can vanish since all points about point 0 can become coplanar, but not collinear. We thus define a criterion δ that indicates the vanishing of an eigenvalue of $\tilde{\mathbf{A}}$ by taking the cube root of the product of its eigenvalues and dividing this by the average of their sum. Thus, we have

$$\delta \equiv \frac{3(\det \tilde{\mathbf{A}})^{\mathbf{1/3}}}{\mathrm{Tr}(\tilde{\mathbf{A}})} < 10^{-3} \frac{\theta \phi}{2\pi^2}. \tag{16}$$

If δ is less than the RHS of the indicated expression above, where θ and ϕ are the effective spherical angles of a given problem in radians, then we do not compute c_j from Eq. (15) but instead calculate these components directly from $\tilde{\mathbf{A}}\mathbf{x} = \mathbf{0}$, as the eigenvector of the zero (or nearly zero) eigenvalue of $\tilde{\mathbf{A}}$. Now $\hat{c}$ is always well defined.

The coordinate-line surface mesh vectors are modified about the point 0 with respect to the surface with logical index l so that the total gradient operator $\vec{A}_{T,0}$ with respect to this surface, $\vec{A}_{T,0} \equiv \sum_{i=1}^{n=4} \vec{A}_{i,0}$ as seen from Fig. 3, has no component in the direction perpendicular to $\hat{c}$. To this end we define the component of this vector that is perpendicular to the direction $\hat{c}$, denoted as $\vec{A}_{\perp,0}$, by

$$\vec{A}_{\perp,0} \equiv \sum_{i=1}^{n} \vec{A}_{i,0} - \sum_{i=1}^{n} (\vec{A}_{i,0} \cdot \hat{c})\, \hat{c}. \tag{17}$$

To remove this component from $\vec{A}_{T,0}$ we simply subtract equal portions of it from each of the vectors $\vec{A}_{i,0}$. Thus, the modified coordinate-line surface mesh vectors that we label as

$\vec{A}^M_{i,0}$ are given by

$$\vec{A}^M_{i,0} = \vec{A}_{i,0} - (\vec{A}_{\perp,0}/n)\,\chi(0), \tag{18}$$

where $\chi(0)$ is a function of point 0, defined in Section 6, that has a magnitude between zero and unity. It is used to decide how much the vector $\vec{A}_{i,0}$ should be modified. It is important to note that although the vector $\vec{A}^M_{T,0} \equiv \sum_{i=1}^{n} \vec{A}^M_{i,0}$ has no component perpendicular to the direction $\hat{c}$ when $\chi(0) = 1$, each modified surface vector $\vec{A}^M_{i,0}$ generally has a nonzero component in this direction. It is only the net sum of these vectors about point 0 that has been eliminated. This is why this modification does not cause egregious changes to the original gradient operator. It is a subtle manipulation of the truncation error of the difference scheme in favor of spherical symmetry, and thus does not impose it when physically absent.

Finally, the median mesh vectors $\vec{S}_{i,0}$ midway between two l-surfaces are also modified in the same manner as that prescribed by Eqs. (17), (18). This is necessary for obtaining symmetry when subzonal pressure forces, or forces due to deviatoric stresses, are discretized. In this case the direction vector $\hat{c}$ used to modify these median mesh vectors is found by simply adding the two $\hat{c}$ vectors from the adjacent l-surface points and renormalizing the magnitude to unity.

5. CALCULATION OF FORCES

It is now assumed that both the coordinate-line and median meshes along the designated l-surfaces have been modified with respect to the local direction $\hat{c}$ by means of Eqs. (15)–(18). These surface areas are designated as $\vec{A}^M_i$ ($\vec{A}_i$ if unmodified) when referring to the coordinate-line mesh, and as $\vec{S}^M_i$ ($\vec{S}_i$ if unmodified) when referring to the median mesh, of a zone z (the subscript for point 0 is hereon suppressed). How the various forces that appear in our model are computed with respect to these two meshes is now detailed. The computation of the corner force vector $\vec{f}^{\,p}_z$ with respect to zone z and point p is given for pressure and material strength forces. The edge-centered artificial viscosity force contribution to $\vec{f}^{\,p}_z$ is calculated from the unmodified median mesh vectors $\vec{S}_i$ as given in the Appendix of [4]. (There are twelve separate viscosity force contributions from a hexahedral zone.) The corner forces are summed over z about a fixed p to obtain the total force $\vec{F}_p$ used to advance velocity in Eq. (4). They are also used to compute the rate of change in internal energy as $-\sum_p \vec{f}^{\,z}_p \cdot \vec{v}^{\,n+1/2}_p$ in Eq. (5). Although the zones may be polygons of any construction, the specific case of hexahedrons is singled out. The generalization of $\vec{f}^{\,p}_z$ to the former case is apparent.

5.1. *Pressure Forces*

The corner force $\vec{f}^{\,p=0}_z(\mathrm{mp})$ due to the mean zone pressure "mp" in zone z that acts on a point $p = 0$ is computed using the coordinate-line mesh subsurface vectors $\vec{A}_i$ that are associated with this point and zone; they are outwardly directed with respect to the volume contained in zone z. For a subzonal corner that is a quadrilateral there are three such vectors as shown in Fig. 4; thus this force is

$$\vec{f}^{\,p=0}_z(\mathrm{mp}) = P_z\big(\vec{A}_1 + \vec{A}_2 + \vec{A}^M_3\big), \tag{19}$$

where P_z is the mean pressure in zone z. The vector $\vec{A}^M_3$ lies along the l-surface of the

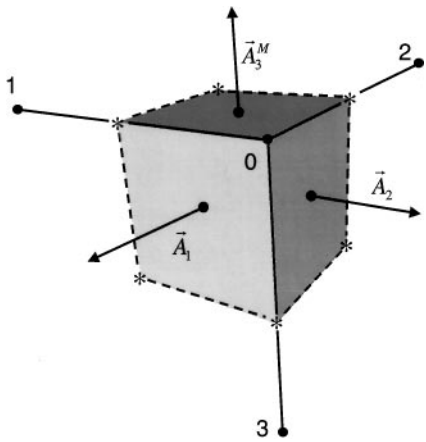

FIG. 4. Coordinate-line mesh corner stencil used for computing mean zone pressure forces. $\vec{A}_3^M$ has been modified for symmetry purposes.

point $p = 0$ and the zone z and has been modified by means of Eq. (18). By defining the direction of the $\vec{A}_i$'s as outward normals, Eq. (19) gives a control volume representation of the integral of the pressure force $-\nabla P_z$ when summed over all zones about point p. Before modification of the vector $\vec{A}_3^M$ for symmetry, this force could be calculated from the median mesh vectors with inwardly directed normals with respect to the nodal volume about point p yielding the identical net result. However, once the symmetry modification has been made these two prescriptions are no longer equivalent. It is only the coordinate-line mesh prescription that can be modified so that symmetry is preserved [2].

The continuity equation is employed to write both the momentum and internal energy equations in Lagrangian form where the density ρ appears outside of the total time derivative of both $\vec{v}_p$ and e_z [3, 1]. Thus, on a spatially staggered grid, for this algebraic step to be valid one must define not only a conserved zone mass M_z, and associated zone density and volume evolution equations, but also a conserved point mass M_p, and point density and volume evolution equations in an analogous manner. This latter step is of crucial importance in that by then considering the spatial interrelation of M_z and M_p by means of the common corner mass m_z^p, one concludes that m_z^p must also be a constant, Lagrangian mass [3]. This leads to the formulation of subzonal pressure forces that stabilize the grid against spurious motions and prevent all grid overlap and tangling. Consequently, there is a different density, and thus pressure, in each zone corner (eight pressures in a hexahedral zone). The differencing of the forces due to these separate internal zone pressures is discussed at length in [3]. This differencing is constrained by the requirement of conservation of momentum, but is not unique. However, when symmetry preservation is also required, only one force differencing is possible. The subzonal corner pressures are subtracted from the mean zone pressure and treated as perturbations. This allows for a larger dynamic range through the introduction of a merit factor, $2M_f$, as defined in [3], that is generally of order unity or less. These forces are small compared to the mean zone pressure forces throughout most of any computation. They become large to resist grid tangling, since if the corner volume of a zone becomes small its subzonal density, and thus pressure, becomes large. This produces forces that strongly resist grid collapse as well as spurious and unresolved grid motions, the latter often referred to as "hourglass" modes.

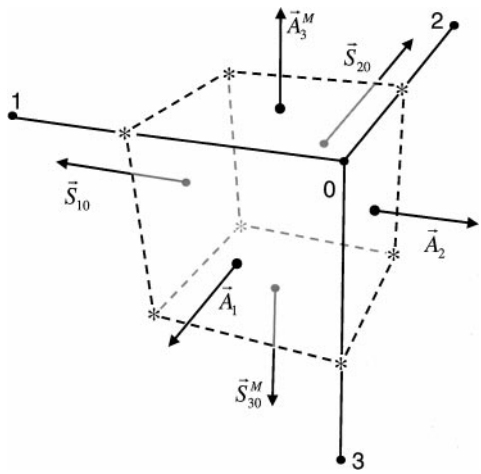

FIG. 5. Coordinate-line and median mesh stencil of a zone corner about point 0 used for computing both subzonal perturbed pressure forces, and material strength forces from subzonal corner deviatoric stresses. Vectors $\vec{A}_3^M$ and $\vec{S}_{30}^M$ have been modified for symmetry.

The subzonal corner perturbed pressure "pp" force $\vec{f}_z^{\,p=0}(\text{pp})$ at point $p=0$ of zone z is computed for a hexahedral zone as

$$\vec{f}_z^{\,p=0}(\text{pp}) = (2M_f)\Big[\delta P_0\big(\vec{A}_1+\vec{A}_2+\vec{A}_3^M\big)+\frac{1}{2}(\delta P_0-\delta P_1)\vec{S}_{10} + \frac{1}{2}(\delta P_0-\delta P_2)\vec{S}_{20}+\frac{1}{2}(\delta P_0-\delta P_3)\vec{S}_{30}^M\Big], \tag{20}$$

where the coordinate-line mesh vectors $\vec{A}_i$, and the median mesh vectors $\vec{S}_i$, are specified as shown in Fig. 5. The first term on the RHS of Eq. (20) is the same as the corner pressure force from the mean zone pressure as given by Eq. (19); the other three terms are force contributions from the median mesh, where $1/2$ of the total force on each median mesh segment is allocated to each of the two grid points involved. The vectors $\vec{A}_3^M$ and $\vec{S}_{30}^M$ have both been modified so that symmetry will be preserved if present in the computation. The contributions from the median mesh vectors $\vec{S}_{10}$ and $\vec{S}_{20}$ are both zero in this case, since when symmetry is present all perturbed corner pressures are equal along an inner or an outer portion of an l-surface. It is for this reason that this force differencing preserves symmetry when present, and it is unique in this sense [3]. The perturbed subzonal corner pressures in a zone, δP_i, are computed by $\delta P_i = c_{s,z}^2(\rho_i-\bar{\rho})/\gamma$, where ρ_i is the subzonal corner density calculated from the Lagrangian subzonal mass and $\bar{\rho}$ is the mean zone density calculated from the Lagrangian zonal mass: $c_{s,z}^2$ and γ are the zone sound speed and the ratio of specific heats of the zone material, respectively.

In computing the timestep that is utilized in our calculations the effects of the mean zone pressure and the artificial viscosity are combined. The scalar part of the artificial viscosity has the form $\rho_i C_i^2$ along every edge i of a zone z [4], where C_i^2 is an effective viscous sound speed squared. The maximum value of all C_i^2 in a given zone is added to the actual zone sound speed $c_{s,z}^2$, as determined from the equation of state. The square root of this sum determines a generalized sound speed that is used to compute the CFL condition for the zone; the minimum of this time for all zones determines the timestep. The time integration

scheme consists of an initial predictor step that advances all dependent variables from time level n to time level $n+1$; this is followed by a single corrector step with forces re-centered at the $n+1/2$ time level.

5.2. *Material Strength Forces*

The construction of forces that arise from material strength presents unique difficulties if one wishes to preserve the limit of 1D spherical symmetry. The first task is to calculate the velocity gradient tensor $\nabla_i v_j$ (defined in the zones) from which the traceless, symmetric strain rate tensor $\epsilon_{i,j}$ is constructed ($\epsilon_{i,j} = [\nabla_i v_j + \nabla_j v_i]/2 - \delta_{i,j} \nabla \cdot \vec{v}/3$). Then the zone deviatoric stress tensors $\overline{\overline{T}}$ can be advanced in time [8]. (For a purely elastic material $T^{n+1}_{i,j} = T^n_{i,j} + 2G\epsilon_{i,j}\Delta t$, where G is the shear modulus). The corner force that is applied to a point from a given zone is then just $\vec{f}^{\,p}_z = -\overline{\overline{T}} \cdot \vec{A}$, where $\vec{A}$ is the total outward normal area vector of a corner volume of zone z with respect to point p. (For a hexahedron this is composed of three coordinate-line mesh vectors, as shown in Fig. 4.)

As was noted in Section 3, the divergence of the velocity calculated in the zones by means of our standard control volume differencing is consistent with 1D spherical symmetry, given a velocity field that is spherically symmetric. With respect to forces that originate from material strength, this requirement is that the eigenvalues of the tensors $T_{i,j}$ or $\epsilon_{i,j}$ all be equal between two l-surfaces (this is equivalent to a symmetric pressure), and that two of these eigenvalues be equal to each other (degenerate and $-1/2$ the value of the third). The eigenvectors of the degenerate eigenvalues define a plane to which the third is the outward normal. For the zones inside two l-surfaces these tensors can be transformed into each other by a similarity transformation and are thus all equivalent. This is the requirement that must be satisfied for the 1D spherically symmetric limit to be attainable by our 3D numerical discretization. Unfortunately, we find that if we directly compute the strain rate tensor $\epsilon_{i,j}$ using 3D control volume differencing, and with a spherically symmetric velocity field defined at the points, that the eigenvalues of $\epsilon_{i,j}$ inside two l-surfaces are not equal to roundoff error, and the curl of the velocity field (anti-symmetric part of $\nabla_i v_j$) is not zero. This is unlike the case of 2D Cartesian geometry [2] where control volume differencing results in these conditions preserved to roundoff error level for an angular grid. Since the divergence of the velocity is consistent with symmetry (a consequence of its being constrained by the volume relation Eq. (7)), it is still possible to obtain the symmetric 1D limit with 3D control volume differencing. This is because the material strength forces in 1D appear as an addition to the forces deriving from the symmetric scalar pressure, and thus the compatible heating resulting from them (and computed using Eq. (5)) will be symmetric. The first problem is that we must construct an alternative to control volume differencing to calculate the strain rate tensor $\epsilon_{i,j}$, and the resulting stresses $T_{i,j}$, that will yield symmetric eigenvalues, and a velocity field with zero curl, to roundoff error.

The solution to the problem just stated is to calculate the deviatoric stresses and the strain rates in subzonal corners (eight tensors per hexahedron instead of one) by means of a finite difference technique that is detailed in the Appendix. These tensors will then have eigenvalues that meet our above stated symmetry requirements. We now assume that these tensors are given and proceed to consider how the corner force that results from them is to be calculated so that the 1D spherically symmetric limit can be achieved.

The proper control volume differencing of forces that are due to subzonal tensors that are piecewise constant in the corner volumes of zones can be constructed in a simple analogy

to how forces are constructed for subzonal pressures. Thus, from Eq. (20), we can simply replace the multiplication of a scalar times a vector by the dot product of a tensor times a vector (also set $2M_f = 1$) to arrive at the corner force acting on point 0 from subzonal material strength ms tensors in zone z as

$$\vec{f}_z^{\,p=0}(\text{ms}) = -\overline{\overline{T}}_0 \cdot \left(\vec{A}_3^M + \vec{A}_1 + \vec{A}_2\right) - \frac{1}{2}(\overline{\overline{T}}_0 - \overline{\overline{T}}_1) \cdot \vec{S}_{10} - \frac{1}{2}(\overline{\overline{T}}_0 - \overline{\overline{T}}_2) \cdot \vec{S}_{20} - \frac{1}{2}(\overline{\overline{T}}_0 - \overline{\overline{T}}_3) \cdot \vec{S}_{30}^M. \tag{21}$$

Once again the coordinate-line mesh vectors $\vec{A}_i$, and the interior zone median mesh vectors $\vec{S}_i$, are directed with outwardly pointing normals to the surface of the subzonal volume in question. Because this sign convention gives $-\nabla \cdot \overline{\overline{T}}$, a minus sign has been inserted into Eq. (21) to achieve the plus sign convention used for computing forces due to deviatoric stresses. The vectors $\vec{A}_3^M$ and $\vec{S}_{30}^M$ are the modified form of these vectors that are used to obtain symmetry for pressure forces. Since $(\vec{A}_3 + \vec{A}_1 + \vec{A}_2) = -(\vec{S}_{10} + \vec{S}_{20} + \vec{S}_{30})$, Eq. (21) (using unmodified vectors) is equivalent to calculating the force as an average of adjacent tensors acting on the median mesh, or

$$\vec{f}_z^{\,p=0}(\text{ms}) = [(\overline{\overline{T}}_0 + \overline{\overline{T}}_1) \cdot \vec{S}_{10} + (\overline{\overline{T}}_0 + \overline{\overline{T}}_2) \cdot \vec{S}_{20} + (\overline{\overline{T}}_0 + \overline{\overline{T}}_3) \cdot \vec{S}_{30}]/2, \tag{22}$$

and thus is a valid contour integral calculation of the force due to these tensors. The remaining question is whether or not the force differencing given by Eq. (21) results in symmetry. This we examine next.

The deviatoric stress tensor $\overline{\overline{T}}_0$ common to point 0 and to zone z as computed in the Appendix can be written in diagonal form as

$$\overline{\overline{T}}_0 = \begin{bmatrix} \lambda\, \hat{c}_0\hat{c}_0 & 0 & 0 \\ 0 & -\lambda/2\, \hat{c}_{0\perp}\hat{c}_{0\perp} & 0 \\ 0 & 0 & -\lambda/2\, \hat{c}_{0\perp'}\hat{c}_{0\perp'} \end{bmatrix}, \tag{23}$$

where we use dyadic notation; the unit vector $\hat{c}_0$ coincides with the outward normal to a sphere fit through point 0 and its nearest neighbors, as given in Section 4, when spherical symmetry is present. The two vectors $\hat{c}_{0\perp}$ and $\hat{c}_{0\perp'}$ are perpendicular to this vector and define the plane of the degenerate eigenvalues $-\lambda/2$. Since all tensors $\overline{\overline{T}}$ common to a given side of an l-surface have these same eigenvalues (but different eigenvectors) when symmetry is present, we can examine Eq. (21) to see if forces at point 0 are aligned with the direction of $\hat{c}_0$. It is clear that both the first and fourth terms on the RHS of this equation meet this requirement. ($\vec{A}_1$ and $\vec{A}_2$ lie totally in regions where the surrounding $\overline{\overline{T}}$'s are identical; $\overline{\overline{T}}_0$ and $\overline{\overline{T}}_3$ are along a common (k, m)-line and have the same eigenvectors.) However, it is not obvious that the second and third terms of Eq. (21) that represents the interaction with the two sides of the median mesh not along $\hat{c}_0$ will yield forces in this direction. Indeed, recall that for subzonal pressure forces these terms vanish because the pressures on either side of $\vec{S}_{10}$ or $\vec{S}_{20}$ are equal. Here the eigenvalues of the tensors on either side of these vectors are equal, but their eigenvectors are different so that this term yields a nonzero force. To examine this we explicitly compute the second term on the RHS of Eq. (21) for the total force exerted on the piece of the median mesh $\vec{S}_{10}$ (we set the

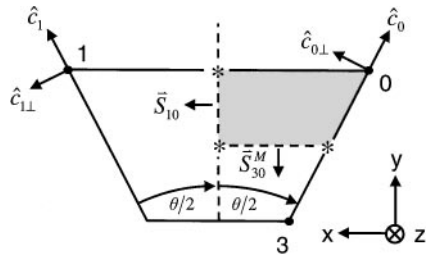

FIG. 6. Planar zone used to calculate subzonal material strength forces along median mesh edge $\vec{S}_{10}$; angle θ is arbitrary.

factor of one-half to unity). This force can be analyzed using a local coordinate system, as indicated in Fig. 6. Since there are two degenerate eigenvalues to all $\overline{\overline{T}}$'s, we need only one perpendicular vector to each $\hat{c}$. The orientation of the median mesh vector $\vec{S}_{10}$ is chosen as $\vec{S}_{10} = (a, 0, 0)$, where "(x, y, z)" defines the respective local Cartesian components of any vector. From Fig. 6 we also have the relevant unit vectors $\hat{c}_0 = (-\sin\theta/2, \cos\theta/2, 0)$ and its normal $\hat{c}_{0\perp} = (\cos\theta/2, \sin\theta/2, 0)$, as well as the vectors $\hat{c}_1 = (\sin\theta/2, \cos\theta/2, 0)$ and $\hat{c}_{1\perp} = (\cos\theta/2, -\sin\theta/2, 0)$ that are necessary for the specification of $\overline{\overline{T}}_1$ ($\hat{c}_0 \to \hat{c}_1$, etc., in Eq. (23)).

Given the above definitions and using Eq. (23), the total force on $\vec{S}_{10}$, denoted as $\vec{F}_{\vec{S}_{10}}$, is given by

$$\begin{aligned}\vec{F}_{\vec{S}_{10}} &= -[(\overline{\overline{T}}_0 - \overline{\overline{T}}_1)\cdot\vec{S}_{10}\\ &= [-\lambda(\hat{c}_0\cdot\vec{S}_{10})\hat{c}_0 + \lambda/2(\hat{c}_{0\perp}\cdot\vec{S}_{10})\,\hat{c}_{0\perp} + \lambda(\hat{c}_1\cdot\vec{S}_{10})\,\hat{c}_1 - \lambda/2(\hat{c}_{1\perp}\cdot\vec{S}_{10})\,\vec{c}_{1\perp}]. \quad (24)\end{aligned}$$

Using the definitions of the vectors in Eq. (24), it can be written in the equivalent form

$$\begin{aligned}\vec{F}_{\vec{S}_{10}} &= a\lambda[\sin\theta/2\,(-\sin\theta/2, \cos\theta/2) + \sin\theta/2\,(\sin\theta/2, \cos\theta/2) + \sin\theta/2\,(0, \cos\theta/2)]\\ &= 3a\lambda\sin\theta/2\,(0, \cos\theta/2), \quad (25)\end{aligned}$$

where from here on the third index in our vector notation is suppressed; and, we have used that fact that

$$\begin{aligned}\frac{\lambda}{2}[(\hat{c}_{0\perp}\cdot\vec{S}_{10})\hat{c}_{0\perp} - (\hat{c}_{1\perp}\cdot\vec{S}_{10})\hat{c}_{1\perp}] &= a\lambda\cos\theta/2\,(0, \sin\theta/2)\\ &= a\lambda\sin\theta/2\,(0, \cos\theta/2). \quad (26)\end{aligned}$$

Thus, it is seen from Eq. (25) that this force points in the direction of the average of $\hat{c}_0$ and $\hat{c}_1$, and therefore the allocation of one-half of this force to points 0 and 1, as indicated by Eq. (21), will not result in spherical symmetry preservation. However, if we use the vector relation

$$\sin\theta/2\,(0, \cos\theta/2) = \sin\theta/2\left[\frac{1}{2}(\sin\theta/2, \cos\theta/2) + \frac{1}{2}(-\sin\theta/2, \cos\theta/2)\right], \quad (27)$$

then Eq. (25) can be rewritten as

$$\vec{F}_{\vec{S}_{10}} \equiv \vec{F}_{0,\vec{S}_{10}} + \vec{F}_{1,\vec{S}_{10}} = \frac{3a\lambda}{2}[\sin\theta/2\,(-\sin\theta/2, \cos\theta/2) + \sin\theta/2\,(\sin\theta/2, \cos\theta/2)]. \tag{28}$$

Finally, we write the two terms that appear in Eq. (28) as separate forces

$$\vec{F}_{0,\vec{S}_{10}} = -\frac{3}{2}[(\overline{\overline{T}}_0 \cdot \vec{S}_{10}) \cdot \hat{c}_0]\,\hat{c}_0, \tag{29}$$

$$\vec{F}_{1,\vec{S}_{10}} = +\frac{3}{2}[(\overline{\overline{T}}_1 \cdot \vec{S}_{10}) \cdot \hat{c}_1]\,\hat{c}_1, \tag{30}$$

where the first equation is to be added to the corner force applied to point 0, and the second to point 1. This decomposition divides the total force on the median mesh vector $\vec{S}_{10}$ into separate $\hat{c}_0$ and $\hat{c}_1$ directed components and is found to result in symmetry preservation. In the above equations the force $\overline{\overline{T}} \cdot \vec{S}$ due to each tensor is calculated and then projected into the direction of $\hat{c}$ at the point in question. It is seen that the degenerate eigenvalues add an extra factor of one-half that contributes to the force in the symmetry direction. Note that now only $\overline{\overline{T}}_0$ contributes a force to point 0; and likewise, only $\overline{\overline{T}}_1$ contributes a force to point 1.

The above is valid when symmetry is present. However, when symmetry is not present this decomposition, valid for tensors with equal eigenvalues, is not exact, and contributing one-half of the total force from vector $\vec{S}_{10}$ to each adjacent point is a general and convergent prescription. Keeping this in mind we write the total material strength "ms" corner force on point 0 as a combination of Eq. (21) and Eq. (29) using the switch $\chi(p)$ (here p denotes point 0) to obtain

$$\vec{f}_z^{\,p=0}(\text{ms}) = -\overline{\overline{T}}_0\big(\vec{A}_3^M + \vec{A}_1 + \vec{A}_2\big) - \frac{1}{2}(\overline{\overline{T}}_0 - \overline{\overline{T}}_3) \cdot \vec{S}_{30}^M - \frac{1}{2}[(\overline{\overline{T}}_0 - \overline{\overline{T}}_1) \cdot \vec{S}_{10} + (\overline{\overline{T}}_0 - \overline{\overline{T}}_2) \cdot \vec{S}_{20}](1 - \chi(0)) - \frac{3}{2}[\overline{\overline{T}}_0 \cdot (\vec{S}_{10} + \vec{S}_{20}) \cdot \hat{c}_0]\,\hat{c}_0\chi(0), \tag{31}$$

valid for a hexahedral zone and readily extended to arbitrary polygons. The above expression is our final prescription for the corner force due to material strength acting from a zone z to a dynamical point p calculated from subzonal deviatoric stress tensors, one in every corner volume of a zone. Next, the function $\chi(p)$ that automates this and the other correction procedures employed to obtain symmetry is defined.

6. DETERMINATION OF $\chi(p)$

In all of the modifications that have been made to our standard control volume differencing (Eq. (18) for constructing the modified mesh vectors $\vec{A}_i^M$ and $\vec{S}_i^M$, Eq. (31) that defines material strength forces, and Eqs. (38), (39) for computing corner strain rates), the quantity $\chi(p)$, defined on the grid points p has been introduced as a multiplicative factor that ranges in value from zero to unity. This factor determines how much of the corrections necessary to preserve symmetry should actually be retained. The calculation of this factor at each of the grid points is now given by means of an estimation of the variation in the curvature measured between the grid point 0 and its n nearest neighbors.

The curvature vector between two points 0 and i that are on the same spherical surface with a distance vector $\vec{l}_{i0} \equiv \vec{x}_i - \vec{x}_0$ between them is found to be given by

$$\vec{K}_{i0} = \frac{\hat{c}_i - \hat{c}_0}{\vec{l}_{i0} \cdot (\hat{c}_i - \hat{c}_0)/|\hat{c}_i - \hat{c}_0|}. \tag{32}$$

In 2D the vectors $\vec{l}_{i0}$ and $(\hat{c}_i - \hat{c}_0)$ are always parallel when 1D spherical symmetry is present, and the magnitude of $\vec{K}_{i0}$ is equal to the inverse of the spherical radius to roundoff error accuracy. In 3D this is also the case independently of the placement of points if we use the projection of $\vec{l}_{i0}$ along the unit difference vector of $(\hat{c}_i - \hat{c}_0)$, as indicated in Eq. (32). We are interested only in the magnitude of the vectors $\vec{K}_{i0}$. They are first used to construct the mean value of the curvature at point 0. This is defined as $\bar{K}_0 = \sum_{i=1}^{n} |\vec{K}_{i0}|/n$. Next, we construct the root mean square of the deviation of the magnitude of the vectors $\vec{K}_{i0}$ at point 0. This is given by

$$K_0^{\text{rms}} \equiv \left[\frac{1}{n} \sum_{i=1}^{n} \left(\frac{|\vec{K}_{i0}| - \bar{K}_0}{\bar{K}_0} \right)^2 \right]^{1/2}. \tag{33}$$

The quantity K_0^{rms} is zero to roundoff error if the point 0 and its n nearest neighbors all lie on the same spherical surface. Otherwise, it is a positive number that measures the curvature variation about point 0. It is clear that if this number is too large our modifications to obtain a nonexistent spherical symmetry do not make sense and the original scheme should be used about a given point. With this in mind we define the value of $\chi(p)$ at the point $p = 0$ by the set of relations

$$\begin{aligned} &\chi(p=0) = 1.0 && (0 \le K_0^{\text{rms}} \le 0.01), \\ &\chi(p=0) = 1.0 - (K_0^{\text{rms}} - 0.01)/0.09 && (0.01 < K_0^{\text{rms}} \le 0.1), \\ &\chi(p=0) = 0.0 && (0.1 < K_0^{\text{rms}}). \end{aligned} \tag{34}$$

The breakpoints 0.01 and 0.1 in the above expressions are clearly somewhat arbitrary, but ones that we have found to be reasonable. (For an ellipticity of 1.5 and 10° zoning of a 90° quadrant, as in the initial grid for the Schulz ellipse problem in 2D [9], K_0^{rms} varies from 0.025 to 0.14 along an l-line.) The symmetry modifications introduced here should not be used at points about which significant variation in local curvature occurs; if these modifications are used arbitrarily they can be large and lead to a reduction in both robustness and accuracy of the overall differencing scheme. The automation procedure presented gives a dynamically determined, and locally pointwise, way to incorporate corrections that capture symmetry into the framework of control volume differencing in 3D Cartesian, or 2D cylindrical, geometry.

7. NUMERICAL RESULTS

Next are presented a series of numerical examples that are chosen to show the effectiveness of the algorithm developed herein. This effectiveness is measured in terms of both the ability to preserve 1D spherical symmetry when present, and to perform robustly while retaining accuracy when symmetry is absent. All work is calculated compatibly using Eq. (5) so that total energy is always conserved at roundoff error level. Unless otherwise noted, an ideal gas equation of state with $\gamma = 5/3$ is utilized. The artificial viscosity always uses standard

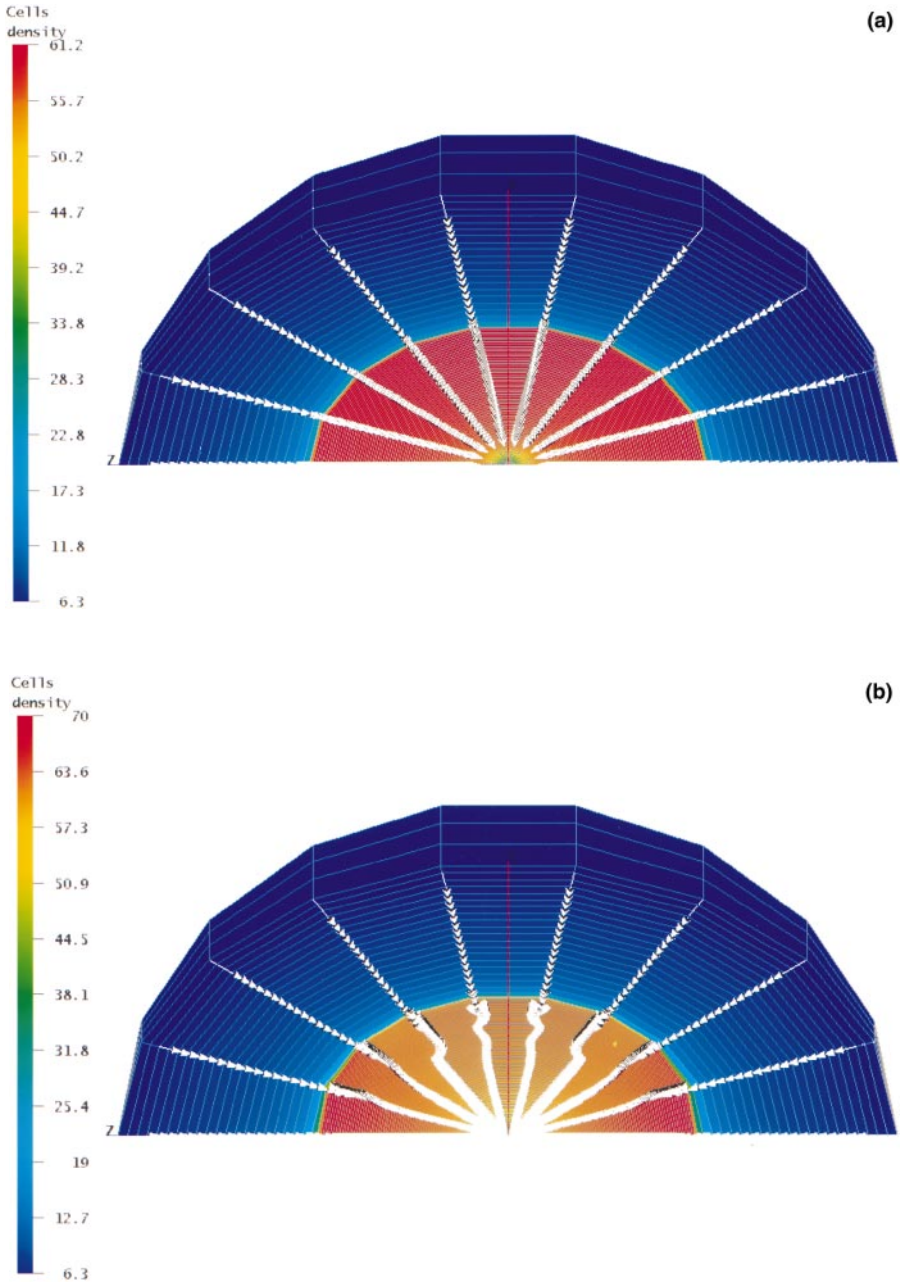

FIG. 7. (a) Noh's problem. Spherical wedge with angles $\Delta\theta = 20^\circ$ and $\Delta\phi = 5^\circ$, density and velocity vectors at $t = 0.6$. Symmetry modification on. (b) Noh's problem. Spherical wedge with angles $\Delta\theta = 20^\circ$ and $\Delta\phi = 5^\circ$, density and velocity vectors at $t = 0.6$. Symmetry modification off.

parameter settings [4]. When the symmetry preserving corrections to the algorithm are turned on it is always in conjunction with the automation factor of Section 6; thus, these corrections are dynamically adjusted. Although the algorithm constructed in this paper can be used with an unstructured grid, all problems are run on a test code that is constructed using a 3D, logically connected grid.

7.1. *Noh's Problem*

Noh's problem [10] is initialized as a sphere of radius unity, with a density of unity, a specific internal energy of zero, and a velocity field that is directed radially inward with a magnitude of unity. A shock wave moves outward from the center of the sphere where the velocity is initially discontinuous. The density inside this outward moving shock wave should have a value of 64.0 and the specific internal energy should be 0.5. At time $t = 0.6$ the shock wave should be at a major radius of 0.2.

In Fig. 7a the density contours with grid and velocity vectors (white heads and black tails) are shown at $t = 0.6$. The grid shown is a spherical wedge of 180° in θ with angles spaced at 20°, and with 15° in angle ϕ using three 5° zones; reflective boundary conditions are specified at planes $\phi = 0^\circ$ and $\phi = 15^\circ$. There are 101 equally spaced l-surfaces at the initial time. The wedge is displayed at 45° with respect to the viewer so that the outer l-surface can be clearly seen. The symmetry modification of Section 4 is turned on. Perfect symmetry of the density and specific internal energy is observed (roundoff error level $\approx$10 decimal digits), and the velocity vectors are perfectly radial. The density rises to about 61.2 with the shock front at about 0.21 at this time. The usual overheating difficulty at the center that is unavoidable with this problem is visible. Figure 7b shows the result for this problem with the corrections for symmetry turned off. The distortions of both the density contours and velocity vectors are clearly seen. The density rises to a value of 70 in some places due to grid distortion.

7.2. *Self-Similar Implosion*

This problem has an analytical solution; it has been studied by numerous authors [11–13]. A sphere with initial unit radius, unit density, and zero internal energy is driven by an inward radial velocity that is specified at the boundary. This radial velocity has a time dependence that is calculated from a self-similar solution expressed as the answer to an ODE problem [13]. An approximate form for this expression as well as the radial density profile at time $t = 0.8$ is given in [2]. The shock converges at the origin of the sphere at $t = 0.75$ and the density should be flat at about 9.5; at $t = 0.8$ the outward propagating radial shock should be at a radius of about 0.11, and with a density peak of 31.5. We employ a grid with 101 l-surfaces. The outer 90 intervals are equally spaced in radius, while the inner 10 are increased in size by a constant factor of 1.05 (ratio zoning). We use 30 angles in the interval $0 \le \theta \le \pi$ whose spacing is determined by choosing equal intervals in $\cos\theta$; two 15° angles in ϕ are used to form a 30° wedge. The nonuniform adjustments in the grid are utilized to keep the timestep from decreasing too much in the course of the simulation. Reflective boundary conditions are applied on the $\phi = 0^\circ$ and $\phi = 30^\circ$ planes. Modifications to obtain symmetry are turned on.

The grid and density contours of this simulation at time $t = 0.8$ are shown in Fig. 8a. A density peak of 32.5 is achieved at a radius of about 0.1, very close to the known solution.

Spherical symmetry is preserved to the level of roundoff error. The central region of the x–z plane of this result is shown in enlarged form in Fig. 8b. Next, this same simulation is run with the symmetry corrections turned off. The grid with density contours in the x–z plane, and enlarged about the center of convergence, is given in Fig. 8c. Here the subzonal pressure forces are still on, but we note the substantial grid distortion that occurs relative to Fig. 8b. Finally, if this simulation is run without either symmetry correction or subzonal pressure forces the result obtained is shown in Fig. 8d. The grid is extremely distorted and the region inside the $l = 2$ surface is smashed into a pancake-like region. If this simulation is run with symmetry corrections, but without subzonal pressure forces, then the results are essentially identical to those of Figs. 8a, 8b. That is, subzonal pressure forces are not needed to obtain correct results for symmetric problems where the initial grid matches this symmetry. They sometimes (but not always) help maintain grid integrity if symmetry corrections are not used, but are not the solution to the symmetry problem. If the subzonal pressure forces are not also constructed to preserve symmetry, then their use with mean zone pressure forces that are symmetry preserving will substantially damage the solution.

We note that the radial distributions of density for both of the preceding problems are close (three digits) to those published using 2D cylindrical geometry [2, 4] with standard viscosity settings and control volume (as opposed to area-weight) differencing with symmetry modifications.

7.3. *Skewed Piston*

One-dimensional shock tube problems have long been used to assess the robustness and accuracy of numerical schemes in both one and two dimensions. This is extended to three dimensions. Here a piston with a square base of length 0.1 on a side and a height of 1.0 is constructed; 10×10 zones compose its base and 100 zones are used along its height. However, the grid lines of this volume are skewed with respect to each other. The entire grid is specified by the formulas

$$\begin{aligned} x &= .01(l-1) + .01(11-k)(6-m)/5 \sin(.01\pi(l-1)) \qquad \text{for } 1 \le m \le 6, \\ x &= .01(l-1) + .01(k-1)(m-6)/5 \sin(.01\pi(l-1)) \qquad \text{for } 7 \le m \le 11, \\ y &= .01(m-1), \\ z &= .01(k-1), \end{aligned} \tag{35}$$

where the height of this grid is along the x direction, and the ranges of k and l are $1 \le k \le 11$ and $1 \le l \le 101$. A side view is shown in Fig. 9a. Its construction is based on generalizing the Saltzman piston grid in 2D [14, 3] in the following manner: the $m = 1$ surface, shown as the top face of Fig. 9a, is the original 2D, skewed Saltzman grid; this grid is additionally skewed with respect to m-surface number into its opposite parity at the $m = 11$ surface (bottom face and hidden in Fig. 9a). The $m = 6$ surface is thus not skewed at all.

The initial density is unity and specific internal energy is zero. Reflective boundary conditions are applied to the four rectangular sides. At the bottom square face a velocity of unity is specified in the x direction; at the opposite square face the velocity in the x direction is set to zero. The shock wave hits this latter face at time $t = 0.75$; the density should be equal to 4.0 in the singly shocked region and equal to 10.0 in the doubly shocked region that results after $t = 0.75$.

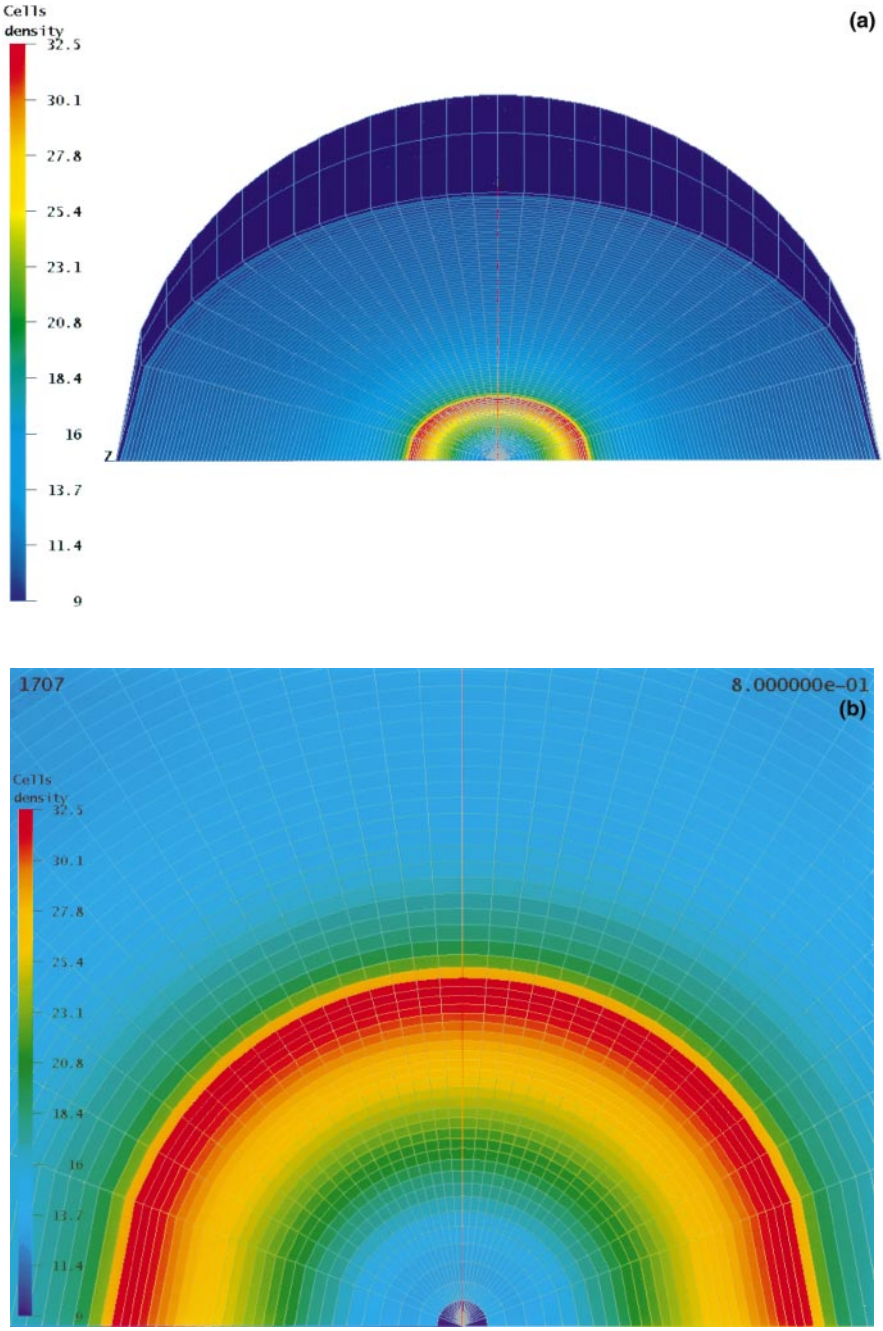

FIG. 8. (a) Self-similar implosion. On-axis center of convergence, density contours, and grid at $t = 0.8$. Symmetry modification on. (b) Self-similar implosion. Density contours and grid at $t = 0.8$ in the x–z plane, enlarged about center of convergence. Symmetry modification on, subzonal pressure forces on with $M_f = 1.0$. (c) Self-similar implosion. Density contours and grid at $t = 0.8$ in the x–z plane, enlarged about center of convergence. Symmetry modification off, subzonal pressure forces on with $M_f = 1.0$. (d) Self-similar implosion. Density contours and grid at $t = 0.8$ in the x–z plane, enlarged about center of convergence. Symmetry modification off, subzonal pressure forces off.

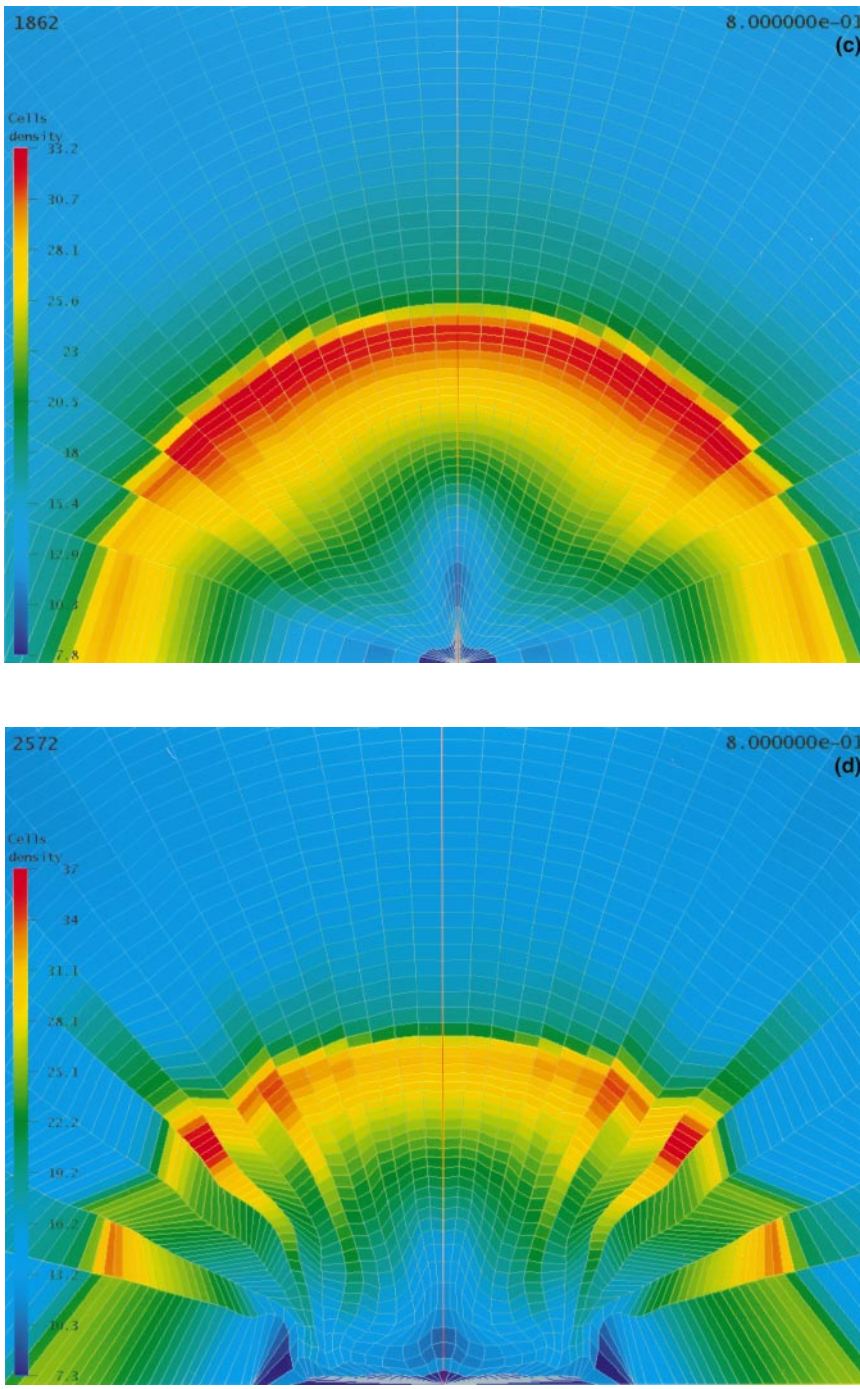

FIG. 8—*Continued*

This problem is run with symmetry modification turned on; the l-surfaces are approximately normal to the flow direction for the initial grid of Eq. (35), so this makes sense. However, the curvature deviation factor K_0^{rms} is found to be about unity over all points of the grid at $t = 0.$, and thereafter in time. Thus, the results shown next are the same as those obtained without this modification. Since the default for this algorithm is to always have the symmetry corrections active, it is important that the automation procedure of Section 6 turn them off continuously as distorted grids develop in time, or are decreed initially.

The grid and density contours of the same two faces visible in Fig. 9a at time $t = 0.0$ are shown in Figs. 9b and 9c at time $t = 0.8$, where in the former case subzonal pressure forces are employed with $M_f = 1.0$, while in the latter case these forces are turned off. The density in the latter case peaks at 23, but is clipped so that an easier comparison can be made. The extreme grid distortion and consequent density perturbations that occur when subzonal pressure forces are not utilized are clearly evident in Fig. 9c, while Fig. 9b shows only very modest grid distortion and density variation from the true solution. Indeed, in this latter case the final grid over which the shock has propagated is mostly straightened out and is much less skewed than the initial grid.

7.4. *Blake's Spherical Elastic Wave*

This problem tests the algorithm when material strength forces (purely elastic in this instance) are present and dominant in determining the solution. The geometry is a hollow sphere with an inner radius of 10 meters that is surrounded by an outer elastic material. A pressure that varies as $p = \exp(-t)$ in time is applied to this inner surface and an elastic wave propagates radially outward [15]. (Units are in (cm/kg/ms) so that pressure is in kb.) The elastic medium has a shear modulus $G = 125$ kb, and an unperturbed density $\rho_0 = 0.002$ kg/cm^3. The equation of state of this elastic medium is given by

$$p = \frac{10^3}{3} \ln\left(\frac{\rho}{\rho_0}\right), \tag{36}$$

and with a constant sound speed of $c_s = 500$ cm/ms.

Our initial grid is constructed using spherical (R, θ, ϕ) coordinates with the inner radius at 10 meters, outer radius at 30 meters, and divided into 80 zones that are 25 cm in length. We choose 45° angular zoning in both θ and ϕ and use two angular zones in each angle to cover one octant of a sphere. Reflective boundary conditions are applied to the $x = 0$, $y = 0$, and $z = 0$ planes of this spherical octant. The problem is run to a time $t = 2.0$ ms. The elastic force contribution is computed in two different ways. First, with all symmetry corrections on the elastic force contribution is calculated from stresses that are defined in corners as detailed in Subsection 5.4, Eq. (31), and with strain rates calculated by the finite difference procedure of the Appendix. Second, with all symmetry corrections off, the elastic forces are computed from zone-centered stresses using zone-centered strain rates calculated from the control volume procedure of the Appendix. In this instance the material strength corner force of Eq. (31) consists of only the first term on the RHS that involves the coordinate-line mesh surface vectors $\vec{A}_i$.

The grid with pressure contours and velocity vectors is shown at time $t = 2.0$ ms for the first case—symmetry corrections on—in Fig. 10a. (This is viewed from behind the origin.) The velocity vectors are radial and the pressure profile exhibits spherical symmetry to

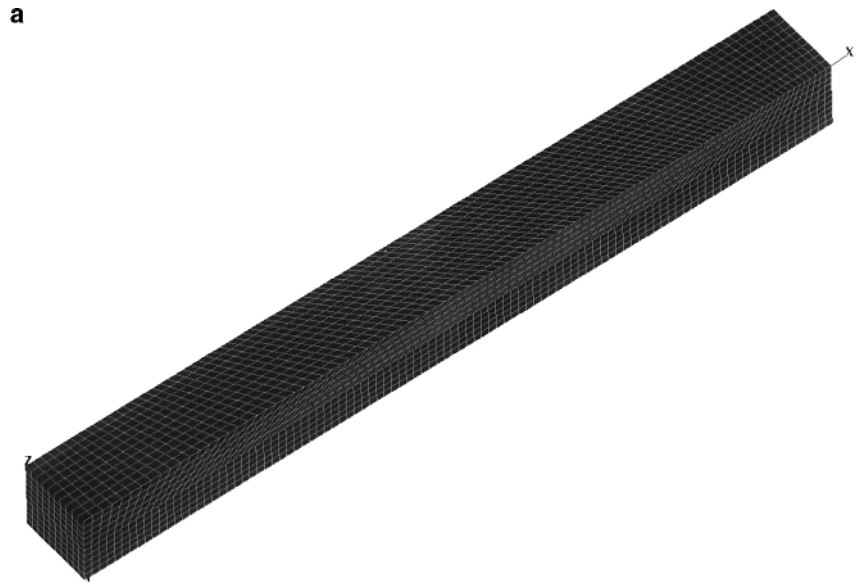

FIG. 9. (a) Skewed piston problem. Initial grid with constant shear along the z direction; faces $z = 0.0$ and $z = 0.1$ (hidden) are skewed with opposite parities but equal magnitudes. (b) Skewed piston problem. Grid and density contours at time $t = 0.8$, subzonal pressure forces on with merit factor $M_f = 1.0$. (c) Skewed piston problem. Grid and density contours at time $t = 0.8$, subzonal pressure forces off.

roundoff error accuracy. The same results for the second case—symmetry corrections off—are displayed in Fig. 10b. Substantial departures from symmetry in both the pressure profile and the velocity vectors that are not along coordinate axes are clearly visible. Since this is basically a wave, the actual grid motion is slight; thus, noticeable grid distortion does not occur and subzonal pressure forces cause negligible changes. The actual grid motion and the velocity profile as a function of radial position is shown in Fig. 10c, along with the analytical solution obtained from Blake [16], for the case where the symmetry preserving algorithm was used. Agreement is seen to be good and can be directly compared to the results given in Fig. 3 of Ref. [15]. With symmetry corrections the results show no sensitivity to the size of the ignorable angles. Without symmetry corrections these results, along various radial grid lines, depart significantly from each other and from the true solution. The solution given by Blake reduces the equations to potential form and thus allows no oscillations of any variables; the comparison here, although close to this solution, is computed with a wave code.

8. CONCLUSIONS

A numerical algorithm has been developed that demonstrates the effectiveness of the Lagrangian description for the numerical solution of problems with moderate to high flow speeds in three-dimensional geometry. The difficulty of anomalous grid distortion and spurious vorticity generation that limits these methods in 2D, and that is expected to be more severe in 3D, is found to be well controlled by the presence of multiple zone pressures that produce stabilizing forces that mitigate this problem. An edge-centered artificial viscosity

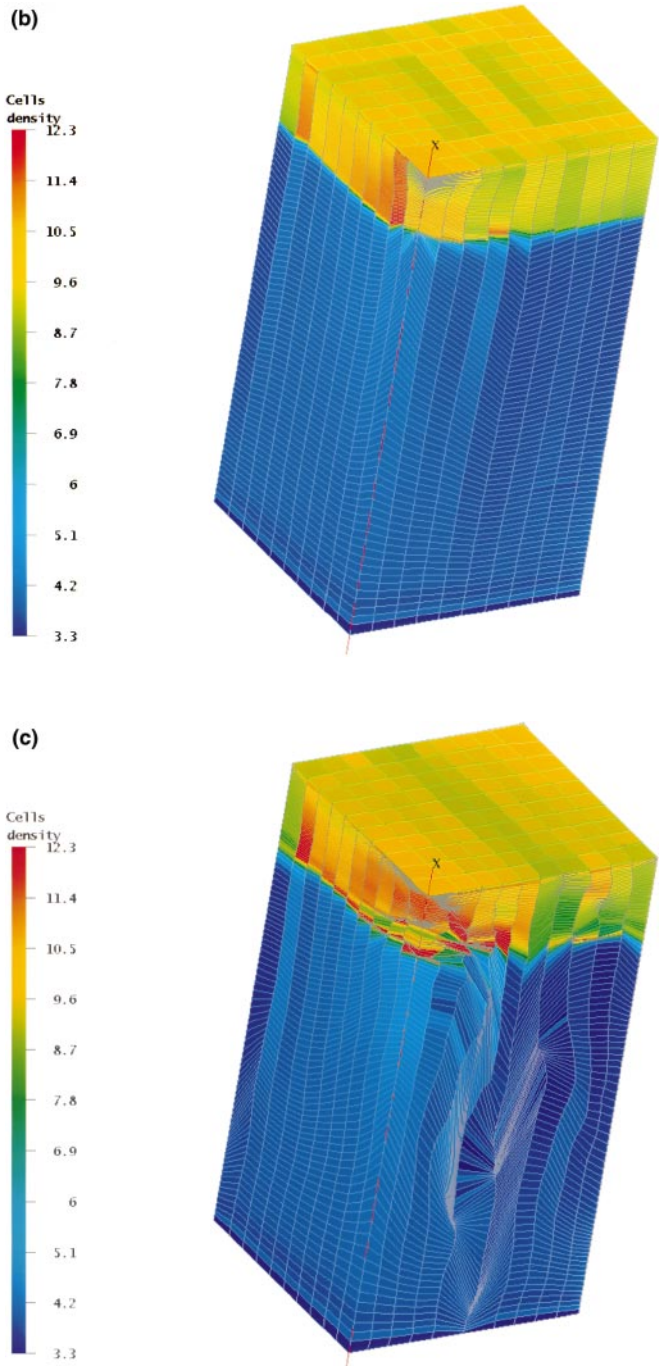

FIG. 9—*Continued*

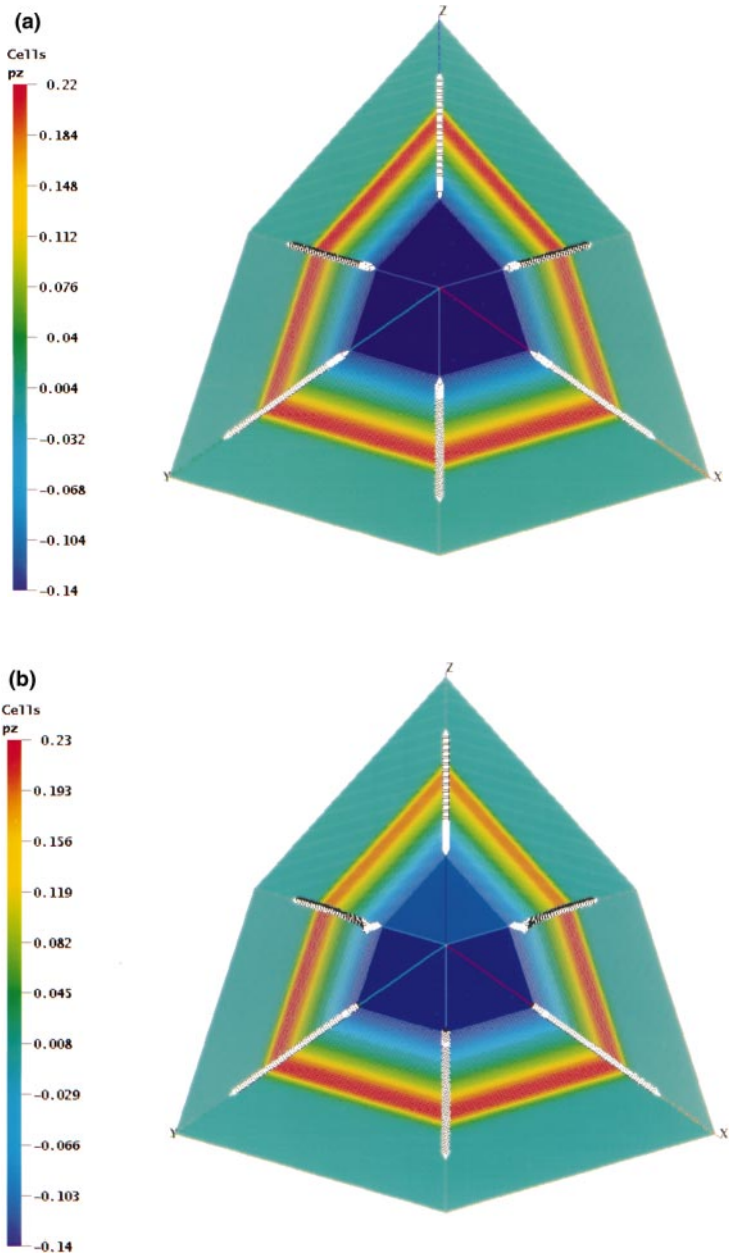

FIG. 10. (a) Blake's elastic expansion wave. One octant of a spherical grid with 45° angles in both θ and ϕ, 25 cm radial zones. Grid with pressure contours and velocity vectors at $t = 2.0$ ms. Symmetry modification on. (b) Blake's elastic expansion wave. One octant of a spherical grid with 45° angles in both θ and ϕ, 25 cm radial zones. Grid with pressure contours and velocity vectors at $t = 2.0$ ms. Symmetry modification off. (c) Blake's elastic expansion wave. Radial distributions of velocity v, and displacement ΔR, at $t = 2$ ms. Solid curves are numerical solution; dashed curves are analytic result. Symmetry modification on.

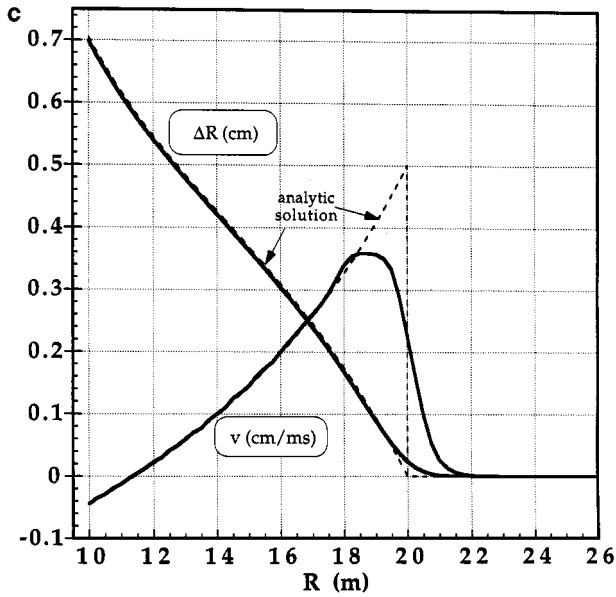

FIG. 10—*Continued*

that is effective in resolving shock disturbances in 3D is utilized. This viscosity, by means of a simple limiter procedure, is able to reproduce the desirable effects of Riemann problem solutions along each edge of each zone without the complexity that the latter entail. The heretofore unsolved problem of perfectly preserving 1D spherical symmetry in 3D Cartesian geometry has been solved by the use of a judiciously chosen set of modifications to the surface vectors that compose the underlying control volume scheme. These changes are automated in such a way that the robustness of the original control volume scheme is not degraded when such symmetry is not a good approximation. This property of the algorithm allows for 3D perturbation studies of spherical problems to be performed without pollution from numerically generated errors—a subject of future work. The framework of compatible differencing has been used to construct this algorithm. This is necessary in order to include the desirable effect of forces that do not have ready continuum analogs that can be directly differenced and also provides a solid mathematical underpinning for this work. Although the Lagrangian description has fundamental limitations in that problems with nearly pure velocity shear (e.g., Kelvin–Helmholtz instability) cannot be simulated, other instabilities such as Rayleigh–Taylor unstable flow can be carried far into the nonlinear regime without premature grid tangling [17]. In addition, the algorithm presented can be used as the Lagrangian step of an overall ALE technique for situations where advection of fluid is essential to an accurate solution.

9. APPENDIX: CALCULATION OF STRAIN RATES

Two different techniques are presented for computing the nine components of the velocity gradient tensor $\nabla_i v_j$ that are needed to advance the material deviatoric stresses in time, and to compute the rotation rate by means of the curl of the velocity field.

9.1. *Control Volume Computation*

Suppose that a given zone is defined by n grid points on which velocity and position are specified, and that this zone has a volume V_z as calculated from subzonal tetrahedralization or some other specified interpolant. Then this zone has n corners each with an outward normal vector $\vec{A}_p$ that is also computed along with the specification of V_z. (In Fig. 4, $\vec{A}_p$ at corner point $p = 0$ is given by $\vec{A}_{p=0} = \vec{A}_1 + \vec{A}_2 + \vec{A}_3$.) Then the control volume computation of the of the nine spatial derivatives of the velocity field defined in zone z is given by

$$\nabla_i v_j = \left(\sum_{p=1}^{n} A_{i,p} v_j \right) \Big/ V_z, \tag{37}$$

where the sum is taken over all corners of zone z and both i, j range from 1 to 3 indicating the x, y, and z components, respectively. This is completely analogous to the vector form of control volume differencing given in 2D in Appendix A of [1].

9.2. *Finite Difference Computation*

In order to compute the strain rate tensor $\epsilon_{i,j}$ in a manner that yields the symmetry condition of uniform eigenvalues in all zones adjacent to a common l-surface, and represents irrotational flow accurately ($\nabla \times \vec{v} = 0$ to roundoff error level), we use the following finite difference procedure to calculate the velocity gradient tensor $\nabla_i v_j$ in each corner of every zone. First, we define three edge vectors that describe a corner that is common to a point 0 and a zone z using points 1–0, 2–0, and 3–0 as shown in Fig. 4. We denote the edge vectors between these three sets of points by $\Delta\vec{x}_1$, $\Delta\vec{x}_2$, and $\Delta\vec{x}_3$, respectively, where $\Delta\vec{x}_1$ and $\Delta\vec{x}_2$ are specified in terms of points 0, 1, 2 that are assumed to lie on a common l-surface. These vectors are defined as

$$\begin{aligned} \Delta\vec{x}_1 &= (\vec{x}_1 - \vec{x}_0) - [(\vec{x}_1 - \vec{x}_0) \cdot \hat{c}_0]\hat{c}_0 \chi(0), \\ \Delta\vec{x}_2 &= (\vec{x}_2 - \vec{x}_0) - [(\vec{x}_2 - \vec{x}_0) \cdot \hat{c}_0]\hat{c}_0 \chi(0), \\ \Delta\vec{x}_3 &= (\vec{x}_3 - \vec{x}_0), \end{aligned} \tag{38}$$

where $\vec{x}_i$ is the position vector of point i. For the two vectors $\Delta\vec{x}_1$ and $\Delta\vec{x}_2$ along an l-surface we subtract off the component that is parallel to the outward normal direction $\hat{c}_0$ at point 0. Thus, $\Delta\vec{x}_1$ and $\Delta\vec{x}_2$ are both perpendicular to $\Delta\vec{x}_3$, but not with respect to each other, when symmetry is present. (Like all other corrections performed to obtain symmetry this is automated by the function $\chi(p)$ as defined in Section 6.) Likewise, we denote the edge velocity vectors as $\Delta\vec{v}_1$, $\Delta\vec{v}_2$, and $\Delta\vec{v}_3$. These are similarly defined by

$$\begin{aligned} \Delta\vec{v}_1 &= (\vec{v}_1 - \vec{v}_0) - [(\vec{v}_1 - \vec{v}_0) \cdot \hat{c}_0]\hat{c}_0 \chi(0), \\ \Delta\vec{v}_2 &= (\vec{v}_2 - \vec{v}_0) - [(\vec{v}_2 - \vec{v}_0) \cdot \hat{c}_0]\hat{c}_0 \chi(0), \\ \Delta\vec{v}_3 &= (\vec{v}_3 - \vec{v}_0). \end{aligned} \tag{39}$$

In our notation $\Delta\vec{x}_1 \equiv (\Delta x_1, \Delta y_1, \Delta z_1)$ and $\Delta\vec{v}_1 \equiv (\Delta v_{1x}, \Delta v_{1y}, \Delta v_{1z})$, etc., as defined above.

Using these vectors we can write three sets of three equations in three unknowns whose solution yields the nine differential components of the velocity gradient tensor in the corner considered. The first set of these, which determine $\partial v_x/\partial x$, $\partial v_x/\partial y$, and $\partial v_x/\partial z$, is written out below as

$$\begin{aligned}
\left(\frac{\partial v_x}{\partial x}\right)_{c,p}\Delta x_1 + \left(\frac{\partial v_x}{\partial y}\right)_{c,p}\Delta y_1 + \left(\frac{\partial v_x}{\partial z}\right)_{c,p}\Delta z_1 &= \Delta v_{1x},\\
\left(\frac{\partial v_x}{\partial x}\right)_{c,p}\Delta x_2 + \left(\frac{\partial v_x}{\partial y}\right)_{c,p}\Delta y_2 + \left(\frac{\partial v_x}{\partial z}\right)_{c,p}\Delta z_2 &= \Delta v_{2x},\\
\left(\frac{\partial v_x}{\partial x}\right)_{c,p}\Delta x_3 + \left(\frac{\partial v_x}{\partial y}\right)_{c,p}\Delta y_3 + \left(\frac{\partial v_x}{\partial z}\right)_{c,p}\Delta z_3 &= \Delta v_{3x},
\end{aligned} \tag{40}$$

where the subscripts (c, p) designate that these derivatives are defined in the corner c of the zone z with respect to point p. By construction these equations are always linearly independent. The additional two sets of three equations are obtained by letting $v_x \to v_y$ and $v_x \to v_z$ in the above. If more than three surface vectors define the corner of a given zone, then the sets of equations given above are over-determined. However, only one vector will lie between l-surfaces ($\Delta\vec{x}_3$ and $\Delta\vec{v}_3$ in the above) so that these sets of equations can be solved by multiplying by their matrix transpose, yielding a well-defined least squares solution.

Given the nine partial derivatives of the velocity gradient tensor calculated as indicated, it is found that for a spherically symmetric velocity field (specified on sets of points distributed in space in a manner consistent with that described in Section 3), that the eigenvalues of $\epsilon_{i,j}$ are equal on a common inner or outer layer of an l-surface, and $\nabla \times \vec{v} = 0$, to roundoff error level. In addition, the eigenvector of the principal eigenvalue of $\epsilon_{i,j}$ defined about point 0 is identical with $\hat{c}_0$. These tensors are thus aligned properly for a force calculation by means of the control volume procedure detailed in Subsection 5.4. Except for initial debugging purposes, the eigenvalues of the tensors $\epsilon_{i,j}$ or $T_{i,j}$ never need to be computed.

ACKNOWLEDGMENTS

We thank M. Shashkov for useful discussions of the computation of velocity gradients, T. Wilson for insights into Blake's elastic wave problem, and L. Margolin for useful comments. This work was supported by the Advanced Strategic Computing Initiative (ASCI) under the auspices of the U.S. Department of Energy.

REFERENCES

1. E. J. Caramana, D. E. Burton, M. J. Shashkov, and P. P. Whalen, The construction of compatible hydrodynamics algorithms utilizing conservation of total energy, *J. Comput. Phys.* **146**, 227 (1998).
2. E. J. Caramana and P. P. Whalen, Numerical preservation of symmetry properties of continuum problems, *J. Comput. Phys.* **141**, 174 (1998).
3. E. J. Caramana and M. J. Shashkov, Elimination of artificial grid distortion and hourglass-type motions by means of Lagrangian subzonal masses and pressures, *J. Comput. Phys.* **142**, 521 (1998).
4. E. J. Caramana, M. J. Shashkov, and P. P. Whalen, Formulations of artificial viscosity for multi-dimensional shock wave computations, *J. Comput. Phys.* **144**, 70 (1998).
5. D. E. Burton, *Multidimensional Discretization of Conservation Laws for Unstructured Polyhedral Grids*, Lawrence Livermore National Laboratory Report, UCRL-JC-118306, August 1994.

6. L. Margolin and M. Shashkov, Using a curvilinear grid to construct symmetry-preserving discretizations for Lagrangian gas dynamics, *J. Comput. Phys.* **149**, 389 (1999).
7. E. J. Caramana, Compatible differencing of slide lines, terminated lines, and exceptional points in Lagrangian hydrocodes, to be published.
8. L. G. Margolin and E. C. Flower, "*Numerical Simulation of Plasticity at High Strain Rate*," LAUR-91-1292 Los Alamos National Laboratory Report, 1991.
9. W. D. Schulz, Two-dimensional Lagrangian hydrodynamic difference equations, *Methods Comput. Phys.* **3**, 1 (1964).
10. W. F. Noh, Errors for calculations of strong shocks using an artificial viscosity and an artificial heat flux, *J. Comput. Phys.* **72**, 78 (1987).
11. G. Guderley, Strarke kugelige und zylindrische Verdichtungsstosse in der Nahe des Kugelmittelspunktes bzw. der Zylinderachse, *Luftfahrt-Forsch.* **19**, 302 (1942).
12. K. P. Stanyukovich, *Unsteady Motion of Continuous Media* (Academic Press, New York, 1960), p. 506.
13. R. Lazarus, Self-similar solutions for converging shocks and collapsing cavities, *SIAM J. Numer. Anal.* **18**, 316 (1981).
14. J. K. Dukowicz and B. Meltz, Vorticity errors in multidimensional Lagrangian codes, *J. Comput. Phys.* **99**, 115 (1992).
15. G. Maenchen and S. Sack, The tensor code, *Methods Comput. Phys.* **3**, 181 (1964).
16. F. G. Blake, Jr., Spherical wave propagation in solid media, *J. Acoust. Soc. Am.* **24**, 211 (1952).
17. E. J. Caramana, L. G. Margolin, and V. Mousseau, Mesh stabilization for Lagrangian simulation of solid dynamics of elastic-plastic flow, to be published.